



iJRASET

International Journal For Research in
Applied Science and Engineering Technology



INTERNATIONAL JOURNAL FOR RESEARCH

IN APPLIED SCIENCE & ENGINEERING TECHNOLOGY

Volume: 5

Issue: XI

Month of publication: November 2017

DOI:

www.ijraset.com

Call: ☎ 08813907089

E-mail ID: ijraset@gmail.com

Noval Zn_2SnO_4 -Doped TiO_2 Photoanode for Dye-Sensitized Solar Cells

Mogali¹, Chaitanya²

¹Assistant Professor, Department of physics, Sridevi Women's Engineering College, Vattinagulapally, Gopanally, Hyderabad-500 075

Abstract: Zn_2SnO_4 doped TiO_2 photo anode material general formula of $(100-x) \text{TiO}_2 + x \text{Zn}_2\text{SnO}_4$ ($x=0, 3, 5$ and 7 mol\%) are synthesized by simple solid-state reaction method followed by high-energy ball milling for 20 hours to form the homogeneous nano scaled photo anode material. Zn_2SnO_4 doped TiO_2 photo anode shows improvement of power conversion efficiency of DSSC. Power efficiency and Zn_2SnO_4 nanoparticle distribution output with the increased surface area was investigated by SEM and XRD analysis. After Zn_2SnO_4 doping, the conductivity of the TiO_2 powder enhanced, and its flat-band potential (V_{fb}) has a positive shift. The energy-conversion efficiency of a cell based on 5.0 mol\% Zn_2SnO_4 -doped TiO_2 is significantly better, by about 16.1% , compared to that of a cell based on undoped TiO_2 . Ball milling process exhibited the best performance with optimized solar energy conversion efficiency of 8.83% with fill factor of 0.712 .

Keywords: Solar energy, Dye-sensitized solar cells (DSSC), Zn_2SnO_4 doped TiO_2 , Photo-anode, Ball milling.

I. INTRODUCTION

Dye-sensitized solar cells (DSSC) have been attracting much attention as alternative energy sources for the next generation solar cells due to their low production cost, the relatively high power conversion efficiency (PCE) and ecofriendly production when compared with silicon solar cells [1-2]. Several photo anode materials TiO_2 , ZnO , SnO_2 , Nb_2O_5 , and SrTiO_3 have been studied in developing high-performance DSSC, due to their wide energy band gap ($E_g > 3 \text{ eV}$), good stability against photo corrosion (transparent to the major part of the solar spectrum) and good electronic properties [3-8]. Among them, pure anatase TiO_2 has been proven to be the best photo anode materials due to its abundance, chemical stability and excellent charge transport capability. However, pure anatase TiO_2 faces poor photo anode activity, low absorption in the UV spectrum, low excitation lifetimes and low amounts of dye adsorption.

In recent years, many attempts were made to overcome the limitations of TiO_2 by doping with metal-oxides improve the significance of TiO_2 photoanode material activity. However, doping ZnO/SnO metal-oxides have emerged as an excellent composite for DSSCs. Semiconducting ZnO and SnO nano particles are offering high surface area, high dye adsorption capability, high chemical stability and longer electron lifetime. Bing Tan et al [9] successfully demonstrated Zn_2SnO_4 as photoanode for DSSC. In order to meet the excellent charge transport capability and photoelectric conversion efficiency (η), our choice of interest is to propose a new type of Zn_2SnO_4 doped TiO_2 nano composite as a photo anode material for DSSC.

In this work, we successfully demonstrated efficient improvement of DSSC by addition of Zn_2SnO_4 semiconductor material to TiO_2 photo anode material. Power conversion efficiency of TiO_2 significantly improved by doping Zn_2SnO_4 , due to their lower conduction band and higher electron mobility. It facilitated more efficient electron transfer from excited states of dye molecules to Zn_2SnO_4 doped TiO_2 composite through an external load. The effect of ball milling increases the surface of photoanode materials and enhanced Zn_2SnO_4 dispersion in TiO_2 matrix and the homogeneity in the hybrid composite.

II. EXPERIMENTAL

Zn_2SnO_4 -Doped TiO_2 photo anode material synthesized by taking stoichiometric ratios of analytical reagent grade ZnCO_3 , SnO and TiO_2 were mixed thoroughly and ground in an agate mortar for 30 minutes to form a homogeneous mixture. Then, the mixture is placed in an alumina crucible and annealed at 700°C for two hours in an electric furnace. Further, high energy ball milling method was used for 20 hours to form the homogeneous nano scaled photo anode powder. Each Zn_2SnO_4 -Doped TiO_2 powdered sample (approximately 3 g) was added to 2 ml of absolute ethanol in a sealed container and ball milled overnight. 0.6 ml Acetic acid and a drop of TritonTM X -100 were later added to the slurry and stirred in an agate mortar until viscous enough for pasting onto fluorine doped tin oxide coated (FTO) glass (Nippon sheet glass $10\text{-}12 \Omega\text{sq}^{-1}$) using a microscope glass edge. After drying, an active area of $\sim 0.3 \text{ cm}^2$ was shaped in the center of the conductive glass ($2 \text{ cm} \times 1.1 \text{ cm}$). Prior to pasting, the conductive glass substrates were

washed 4 times using ultra sonication in soapy water, DI water, IPA and acetone for 10 min, respectively. The prepared anodes were then sintered in a furnace at 500 °C for 30 min, to remove all organic additives.

The sintered electrodes were dipped in 0.5 mM N719 dye in ethanol for 12 h at room temperature and later washed with excess ethanol. Each dyed electrode was combined with a Pt-coated glass counter electrode and sandwiched with electrolyte (EL-SGE Electrolyte, DYSOL). The electrolyte was introduced by placing a drop on the active area of the photoanode. Parafilm paper, PM-996, was carefully cut and used as a spacer. A counter electrode was then placed on top of the photoanode, and the electrodes were held firmly together by crocodile clips.

The photocurrent density–voltage (J–V) measurement was tested using a Keithly 2611 Source Meter (Keithley Instruments, Inc.). The light source was an AM 1.5 solar simulator (91160A, Newport Co.). The incident light intensity was 100 mW cm⁻² calibrated with a standard Si solar cell. The tested solar cells were masked to a working area of 0.2 cm². XRD studies carried out by using PAN analytical Diffract meter B.V fitted with Cu target (both K(α1+α2) wavelengths) and Ni filter at 40 kV and 30 mA (2θ range). The crystallite sizes were examined with SEM pictures (Zeiss Gemini 1530 operated at 1kV)

III.RESULTS AND DISCUSSIONS

Fig. 1 shows the X-ray diffraction patterns of the un doped and Zn₂SnO₄-doped TiO₂ with different Zn₂SnO₄ contents. The broad peaks in all the Zn₂SnO₄-doped TiO₂ are well-indexed corresponding to the major crystalline phase anatase (TiO₂) (ICSD Collection code # 9852), structure indexed to Tetragonal/ I 41/a m d space group and minor crystalline phase Zinc Stagnate (Zn₂SnO₄) phase (ICSD Collection code # 24234). This broad peaks clearly indicating that the anatase nano crystalline structure is retained after doping. The diffraction peaks shift to lower theta values with increasing Zn₂SnO₄ content because of the larger radius of Zn²⁺ (0.74 Å) and Sn⁴⁺ (0.69 Å) compared to that of Ti⁴⁺ (0.61 Å), in accordance with the Bragg equation: 2dsinθ = nλ (Fig. 1). Furthermore, the intensity of the diffraction peaks and volume of the unit cell gradually increasing with Zn₂SnO₄ content up to 5 mol%. According to our knowledge, this new approach creates a higher order in the TiO₂ nanoparticles through the Zn₂SnO₄ doping, which makes the particles in favor of electron transfer, resulting in an increased photocurrent. Table I shows calculated and experimental structural parameters of Zn₂SnO₄ doped TiO₂ photoanode materials.

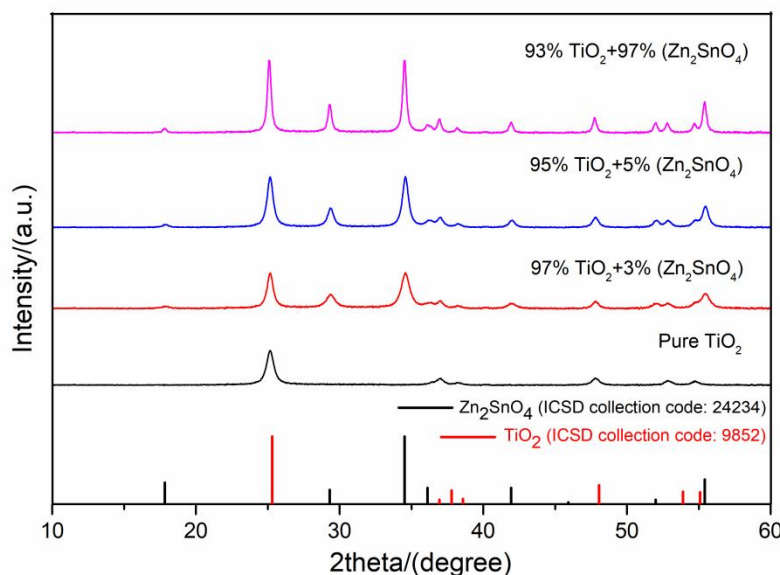


Fig. 1 XRD patterns of Zn₂SnO₄-doped TiO₂ photoanode material.

The crystallite sizes calculated from the Debye-Scherrer equation are listed in Table I, and they are shown to be well consistent with the SEM images shown in Figure 2. The SEM images in Figure 2 indicate the high crystallinity of the TiO₂ nanoparticles. Average crystallite size is achieved to be lowest (~ 120 nm) for 5 mol% Zn₂SnO₄ doped TiO₂ sample (Fig. 2 (c)), which clearly suggested that this sample may create the large electron-holes transfer, resulting in an increased photocurrent. Indeed, uncontrolled agglomeration Sn⁴⁺ particles of crystallites can also be seen in the SEM image of 7 mol% Zn₂SnO₄ sample (Fig. 2(d)). The correlation between the microstructural and electrochemical characterization of these samples will be explained in the next section.

Table I Calculated and experimental structural parameters of TiO_2 doped Zn_2SnO_4 Photo anode materials

Photo anode material	Reference	a (Å)	b (Å)	c (Å)	α ($^\circ$)	β ($^\circ$)	γ ($^\circ$)	Volume [\AA^3]	crystallite size (nm)	Crystal system/ Space group
Experimental	10	3.7840	3.7840	9.5150	90	90	90	136.24		Tetragonal/ I 41/a m d
Pure TiO_2	This work	3.7795	3.7795	9.3444	90	90	90	133.48	200.8 nm	
97% TiO_2 + 3% (Zn_2SnO_4)	This work	3.8023	3.8023	9.7447	90	90	90	140.88	160.1 nm	
95% TiO_2 + 5% (Zn_2SnO_4)	This work	3.8090	3.8090	9.7327	90	90	90	141.21	120.4 nm	
93% TiO_2 + 7% (Zn_2SnO_4)	This work	3.7707	3.7707	9.3461	90	90	90	132.88	260.5 nm	

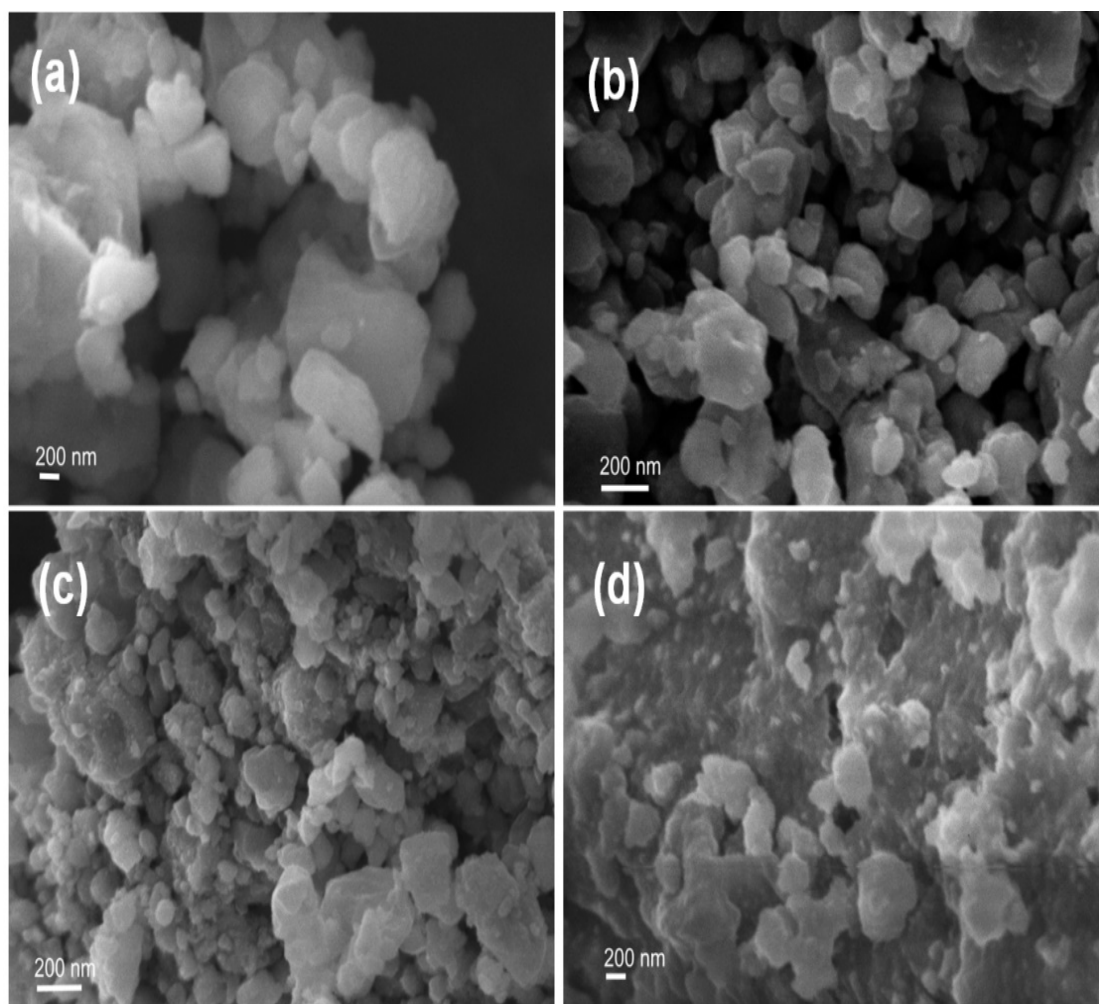

Fig. 2 SEM images of (a) un doped pure TiO_2 (b) 3 mol% (c) 5 mol% (d) 7 mol% Zn_2SnO_4 doped- TiO_2 photo anode materials

Fig. 3 shows average nanoparticle size distribution of SEM images (Fig. 2) of un-doped and Zn_2SnO_4 doped- TiO_2 photoanode materials by using with ImageJ software. These results clearly indicate that the crystalline size of Zn_2SnO_4 doped and undoped TiO_2 photoanode materials decreasing the crystalline size by increasing content of Zn_2SnO_4 up to 5 mol%. The average crystalline size is distributed to ~ 100-300 nm for all samples.

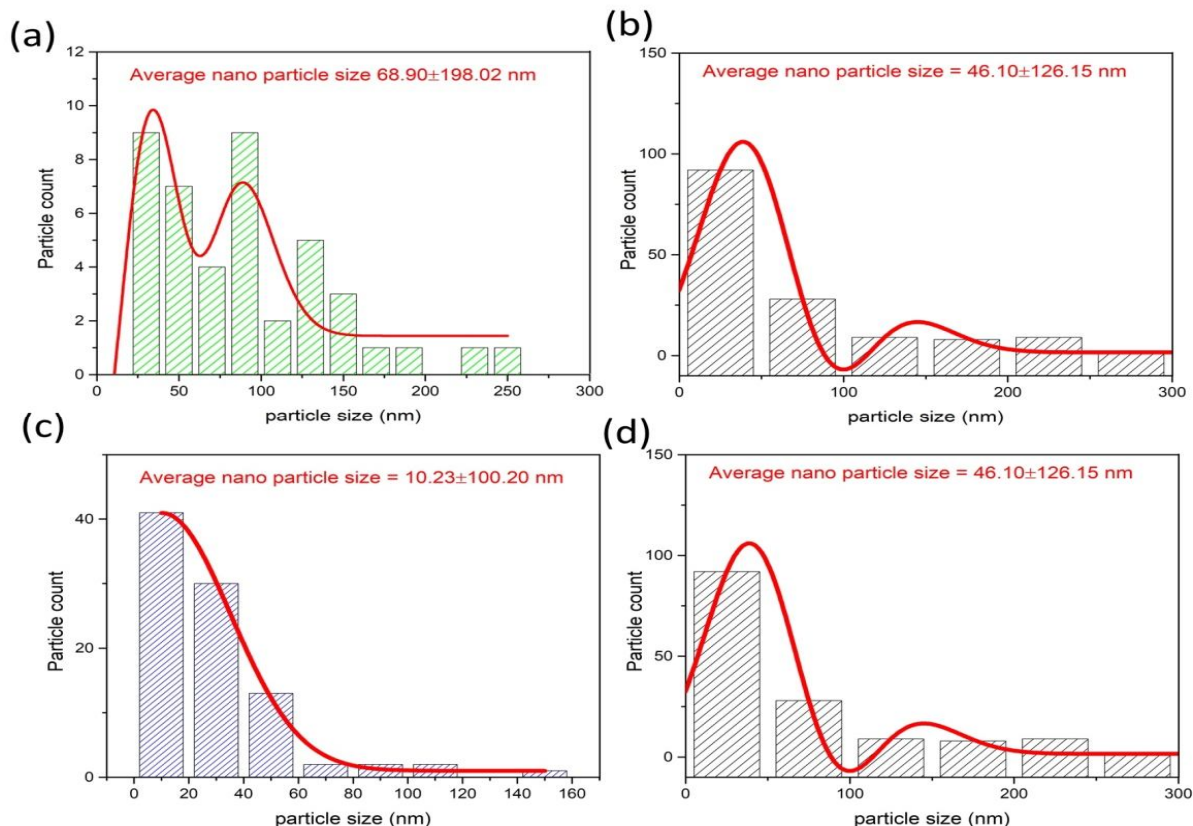


Fig. 3 Particle size distribution of (a) un doped pure TiO_2 (b) 3 mol% (c) 5 mol% (d) 7 mol% Zn_2SnO_4 doped- TiO_2 photoanode material SEM images.

Fig. 4 shows the current density-voltage curves of the open cells based on Zn_2SnO_4 -doped and un doped TiO_2 photoelectrodes. The average performance characteristics obtained from multiple cells with the same Zn_2SnO_4 content are summarized in Table II. The short-circuit photocurrent density (J_{sc}), the open-circuit voltage (V_{oc}) and the photoelectric conversion efficiency (η) increase with the Zn_2SnO_4 -doping to reach a maximum at a $\text{Zn}_2\text{SnO}_4/\text{Ti}$ ratio of at mol % and then decrease. The film thickness and dye-loading amount are similar for both of the photoanode films, indicating that the increase of photocurrent for the Zn_2SnO_4 -doped TiO_2 is not due to the increase in the dye absorption. The higher J_{sc} should result from the enhanced electron transport in the TiO_2 films, which could be explained in the IMPS analysis part. The higher V_{oc} should result from the elevated E_{fb} . With the doping content increases, the concentration of impurities increases. These impurities could act as charge trapping site for the electron-hole recombination. And more serious recombination at high doping content (>5 mol %) could result in a smaller V_{oc} and J_{sc} .

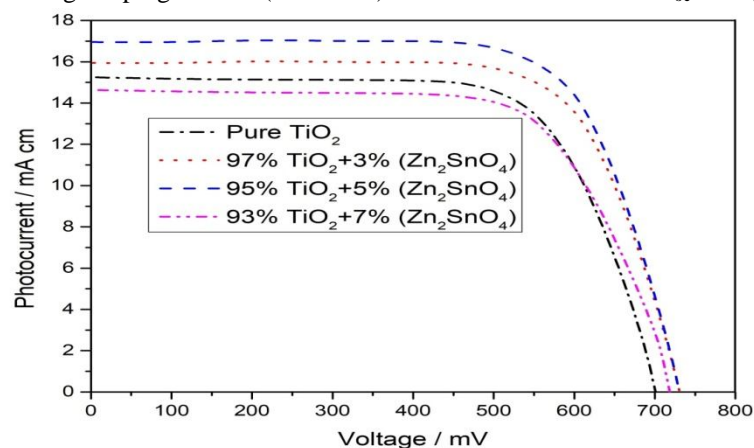


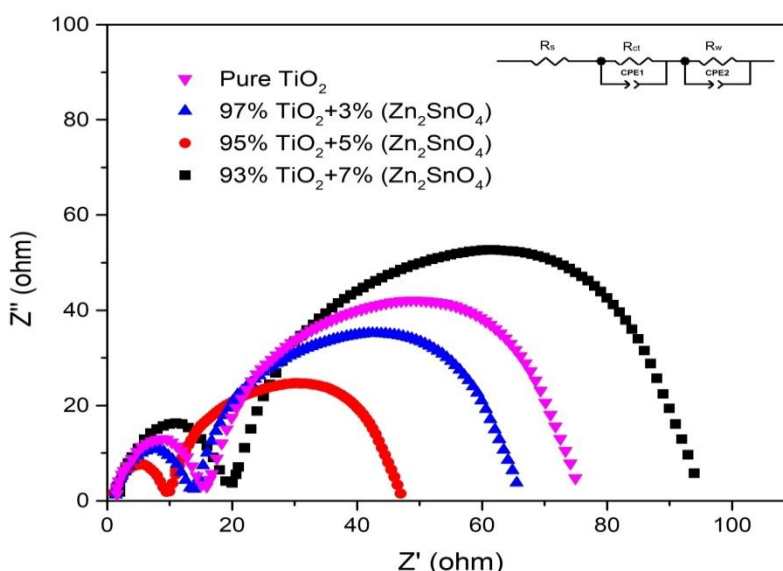
Fig. 4 Current density-voltage (J - V) curves of Zn_2SnO_4 doped- TiO_2 photoanode DSSC.

Table II Photovoltaic Properties of DSSC Assembled with TiO₂ Films of Different Zn₂SnO₄ Contents

DSSC	short-circuit photocurrent (J _{SC}) (mA cm ⁻²)	open-circuit voltage (V _{OC}) (mV)	photoelectric conversion efficiency (η) (%)	Full fill factor (FF)	dye loading (×10 ⁻⁷ mol cm ⁻²)
Pure TiO ₂	15.24	700.64	7.45	0.697	0.99
97% TiO ₂ + 3% (Zn ₂ SnO ₄)	15.94	730.68	8.32	0.714	1.02
95% TiO ₂ + 5% (Zn ₂ SnO ₄)	16.95	730.68	8.83	0.712	0.96
93% TiO ₂ + 7% (Zn ₂ SnO ₄)	14.63	718.41	7.24	0.689	0.97

EIS technique has been widely employed to investigate the kinetics of electrochemical and photo electrochemical process occurring in DSSC. As Shown in Fig. 5, the impedance spectra of DSSCs based on TiO₂ and Zn₂SnO₄-doped TiO₂ films were measured ranging from 1 Hz to 100 kHz. Two semicircles, including a small semicircle at high frequency and a large one at low frequency, were observed in the Nyquist plots of EIS spectra (Fig. 5). As shown in Fig. 5, the small semicircle in the frequency range (<10 Ω) fitted to a charge transfer resistance (R_{ct}) and the Helmholtz capacitance (C_{μ1}) should be ascribed to the charge transfer at the interfaces of the redox electrolyte/Pt counter electrode. The large semicircle in the low-frequency region fitted to a transport resistance (R_w) and the Helmholtz capacitance (C_{μ2}) is related to the charge transfer across either the TiO₂/redox electrolyte interface or the FTO/TiO₂ interface.

According to the EIS model fitted parameters including R_{ct} and R_w obtained by Z view software. Under open circuit condition, no current passes through the external circuit, and the electrons injected into TiO₂ or Zn₂SnO₄-doped TiO₂ are recombined by redox electrolyte at the TiO₂/dye/electrolyte interface. The increased charge recombination found for the Zn₂SnO₄-doped TiO₂ cell could be attributed to higher concentration impurities due to the doping, which acts as a charge trapping site for the electron-hole recombination, hence leading to the decreasing of photon-to-electron conversion efficiency at high Zn₂SnO₄ content (>5 mol %). The Helmholtz capacitance describes the change of electron density under a small variation of the Fermi level. Thus, the value of C_{μ2} gives the total density of free electrons in the TiO₂ conduction band and localized electrons in the trap states. The Zn₂SnO₄-doped TiO₂ film had a smaller capacitance value than the pure-TiO₂ film, which results from the fact that less photogenerated electrons are captured by the empty trap states in the Zn₂SnO₄-doped film due to doping, and this result favors the electron transport.


Fig. 5 EIS spectra of the TiO₂ and the Zn₂SnO₄-doped TiO₂ DSSC

IV. CONCLUSION

In summary, the Zn_2SnO_4 -doped TiO_2 were successfully prepared by simple solid-state reaction method followed by high-energy ball milling under optimized Zn_2SnO_4 content. The best efficiency of 8.83% was achieved by DSSC with 5 mol % Zn_2SnO_4 -doped TiO_2 , which gave an efficiency improved by 16.1% compared with that of the cells based on pure TiO_2 . The DSSC with Zn_2SnO_4 -doped TiO_2 was found to improve the open circuit voltage due to the negative shift of V_{fb} of TiO_2 and enhance the short-circuit current density due to the faster electron transport in the Zn_2SnO_4 -doped TiO_2 films. EIS measurement indicates that the increased charge recombination found for the Zn_2SnO_4 -doped TiO_2 cell could be attributed to high concentration impurities due to the doping, which acts as charge trapping site for the electron-hole recombination, hence leading to the decreasing of photon-to-electron conversion efficiency at the high Zn_2SnO_4 content (>5 mol %). These findings pave a new way to tune the band structure of TiO_2 and improve the charge transport for the high performance of DSSC. Therefore, Zn_2SnO_4 -doped TiO_2 may be developed as a promising photo electrode material for high-efficiency DSSC and other photoenergy conversion devices.

REFERENCES

- [1] L. El Chaar and N. El Zein, "Review of photovoltaic technologies," *Renewable and sustainable energy reviews*, vol. 15, pp. 2165-2175, 2011.
- [2] B. O'regan and M. Grätzel, "A low-cost, high-efficiency solar cell based on dye-sensitized colloidal TiO_2 films," *nature*, vol. 353, pp. 737-740, 1991.
- [3] M. K. Nazeeruddin, F. De Angelis, S. Fantacci, A. Selloni, G. Viscardi, P. Liska, *et al.*, "Combined experimental and DFT-TDDFT computational study of photoelectrochemical cell ruthenium sensitizers," *Journal of the American Chemical Society*, vol. 127, pp. 16835-16847, 2005.
- [4] V. Kumar, N. Singh, V. Kumar, L. Purohit, A. Kapoor, O. M. Ntwaeaborwa, *et al.*, "Doped zinc oxide window layers for dye-sensitized solar cells," *Journal of Applied Physics*, vol. 114, p. 134506, 2013.
- [5] R. A. Jensen, H. Van Ryswyk, C. She, J. M. Szarko, L. X. Chen, and J. T. Hupp, "Dye-sensitized solar cells: sensitizer-dependent injection into ZnO nanotube electrodes," *Langmuir*, vol. 26, pp. 1401-1404, 2009.
- [6] H. J. Snaith and C. Ducati, " SnO_2 -based dye-sensitized hybrid solar cells exhibiting near unity absorbed photon-to-electron conversion efficiency," *Nano letters*, vol. 10, pp. 1259-1265, 2010.
- [7] K. Hara, T. Horiguchi, T. Kinoshita, K. Sayama, H. Sugihara, and H. Arakawa, "Highly efficient photon-to-electron conversion with mercurochrome-sensitized nanoporous oxide semiconductor solar cells," *Solar Energy Materials and Solar Cells*, vol. 64, pp. 115-134, 2000.
- [8] S. Yang, H. Kou, H. Wang, K. Cheng, and J. Wang, "Preparation and band energetics of transparent nanostructured SrTiO_3 film electrodes," *The Journal of Physical Chemistry C*, vol. 114, pp. 815-819, 2009.
- [9] B. Tan, E. Toman, Y. Li, and Y. Wu, "Zinc stannate (Zn_2SnO_4) dye-sensitized solar cells," *Journal of the American Chemical Society*, vol. 129, pp. 4162-4163, 2007.
- [10] E. Meagher, C. Schwerdtfeger, and M. Horn, "Golden Book of Phase Transitions," ed: Wroclaw, 2002.



10.22214/IJRASET



45.98



IMPACT FACTOR:
7.129



IMPACT FACTOR:
7.429



INTERNATIONAL JOURNAL FOR RESEARCH

IN APPLIED SCIENCE & ENGINEERING TECHNOLOGY

Call : 08813907089  (24*7 Support on Whatsapp)